DEFENCE
SCIENCE & TECHNOLOGY

Analysis of a Generic Warhead Part I: Experimental and Computational Assessment of Free Field Overpressure

J.G. Anderson, G. Katselis and C. Caputo

DSTO-TR-1313

DEFENCE
SCIENCE & TECHNOLOGY

Analysis of a Generic Warhead Part I: Experimental and Computational Assessment of Free Field Overpressure

J.G. Anderson, G. Katselis and C. Caputo

Weapons Systems Division
Systems and Sciences Laboratory

DSTO-TR-1313

ABSTRACT

Experimental and numerical results are presented for the free field blast generated by a 7.8 kg cylindrical charge of Composition B high explosive. In the experiments, overpressure and shock front time of arrival measurements have been recorded. Overpressure measurements in the far field provide pressure histories at discrete locations. Peak overpressure in the near field is calculated from time of arrival measurements. In addition, the numerical model was used to generate overpressure histories and two-dimensional contour plots of the blast wave.

RELEASE LIMITATION

Approved for public release

Published by

DSTO Systems and Sciences Laboratory
PO Box 1500
Edinburgh South Australia 5111 Australia

Telephone: (08) 8259 5555
Fax: (08) 8259 6567

AR-012-345
July 2002

APPROVED FOR PUBLIC RELEASE

Analysis of a Generic Warhead Part I: Experimental and Computational Assessment of Free Field Overpressure

Executive Summary

To assist the Royal Australian Navy (RAN) in weapon procurement and platform vulnerability, DSTO is developing an experimental and theoretical capability to assess blast and fragmentation damage mechanisms of anti ship missile defence weapons. Most weapons used in anti-ship missile defence utilise blast/fragmentation warheads. To establish a better understanding of the physics involved, damage mechanisms of blast and fragment impact have been separated. The study presented here focuses on a bare cylindrical blast warhead. This document is the first of two parts. In this report, the analysis of results is for the free field. In the second report, the analysis is extended to blast / target interaction.

Instrumentation employed included blast overpressure, time of arrival sensors and shock front imaging. Cross-correlation of the measurements allowed validation of the different methods employed. A numerical modelling study was conducted concurrently with the experimental investigation. The IFSAS Computational Fluid Dynamics code was used to model the two-dimensional blast profile of the warhead for comparison with experimental measurements. The numerical results showed that a cylindrical warhead can produce a non-uniform blast wave. The maximum overpressure generated by a cylindrical warhead can be significantly higher than an equivalent spherical warhead.

The outcome of this work will lead to a better understanding of the expected level of blast from cylindrical warheads. Ultimately, the aim is to determine the damage to targets and the mechanisms responsible for damage. Future studies will involve pre-formed fragments and fragment / blast synergistic effects. Results of these studies will be added to a database which will be used to develop predictive target damage and vulnerability models for anti ship missile defence.

Authors

J. G. Anderson
Weapons Systems Division

Jeremy Anderson obtained a BE(Mech) Hons in 1996 and completed his PhD in 2000 at Victoria University. He is currently working in the Terminal Effects Group, where his interests include blast/target interaction, fragmentation and fragment impact for vulnerability/lethality assessments.

G. Katselis
Weapons Systems Division

George Katselis obtained a BAppSci in Applied Physics from the Royal Melbourne Institute of Technology (RMIT). He also completed a Ma(Eng) with the Microelectronic Materials and Technology Centre (MMTC) at RMIT in 1995. In 1995-1997 George was employed as a research assistant for Ceramic Fuel Cells Limited where he worked on high temperature oxidation resistant coatings before commencing at DSTO. He is currently working in the Terminal Effects group where he is developing new sensors and instrumentation for measurement of blast and fragmentation effects of warheads and he is also involved in design and experimental analysis of advanced warhead designs.

C. Caputo
Weapons Systems Division

Carmine Caputo obtained a Bachelor of Applied Science - Photography in 1998 at the Royal Melbourne Institute of Technology. He began working at the Proof and Experimental Establishment Port Wakefield in 1999 conducting high speed imaging and analysis of projectiles in flight, and later worked for an automotive crash test facility. He is currently working in the Terminal Effects Group of Weapons Systems Division, where his interests include the development and application of photoinstrumentation, to the study of high speed, short duration explosive events.

Contents

1. Introduction

The detonation of high explosives in air results in an initial localised high pressure and high temperature region. This initial pressure disturbance causes a shock wave in the surrounding air, commonly referred to as the blast wave. It is important to understand the characteristics of blast waves in order to determine the damage capability of conventional weapons and to develop methods to assess potential terrorist attacks or industrial accidents.

Much work has been done to investigate blast and effects of blast against structures. Most of this earlier work focussed on blast waves generated by spherical warheads. Lind et al. [1] investigated the protection of structures from the dynamic loading of blast waves. A numerical study was undertaken to determine the mitigating effects of grid like barriers. The initial boundary conditions of the shock wave were based on a blast wave generated by a spherical warhead of Trinitrotoluene (TNT). Similarly, Ofengeim and Drikakis [2] conducted a numerical study of the interaction of a planar blast wave with cylinders, showing a strong influence of the initial shock conditions on the downstream flow after the cylinder. Varma et al. [3] also used spherical TNT warheads in experiments to provide damage data for brick panel walls.

Ismail and Murray [4] investigated cylindrical warheads and demonstrated that the orientation played a crucial role in the accurate assessment of the blast wave parameters. They found that multiple shocks were present when the warhead axis was in line with the pressure transducer array. Zimmerman et al [5] also investigated the variations between spherical and cylindrical warheads and the effects of various length to diameter ratios. They found that for cylindrical warheads, both peak overpressure and impulse are dependent on the location of the warhead initiation. They also concluded that for high length to diameter ratios more energy is directed in the radial direction and for low length to diameter ratios more energy is directed in the axial direction.

Typically, the blast waves produced from high explosives have been categorised by recording free field static overpressure. This involves measuring the pressure at discrete points in the free field surrounding the explosion. The gauges are usually mounted side-on to the direction of the blast wave. The free field can be loosely divided into three flow regimes, near field, mid field and far field. Recording pressure in the near field is not a trivial exercise. The near field encompasses the fireball and detonation products, making it virtually impossible to measure the peak pressure and the pressure history in this range [6]. Gauges in the near field are exposed to a variety of stimuli and are subjected to many forms of interference. The gauges are sensitive to light, heat and mechanical stresses as well as electromagnetic effects from electrical noise, the firing pulse and from the explosion [7]. Therefore, recording pressure histories at distances of several warhead diameters from the explosive is extremely difficult.

Pressure measurements are generally recorded in the mid to far field. These regions are a sufficient distance from the explosive to ensure that the fireball and detonation products have minimal effect on the pressure gauges. Spherical high explosives will generally create spherical blast waves and pressure measurements in the mid to far field are usually sufficient. However, the blast waves generated by cylindrical warheads differ significantly in the near field [8]. Cylindrical warheads are common in missiles used for anti ship missile defence. Therefore, understanding the characteristics of blast waves produced from cylindrical warheads is important and techniques for determining pressure in the near field are required.

An alternative technique to recording pressure histories in the near field was undertaken. Pressure was not measured directly, rather, the velocity of the blast wave was determined by recording the time taken for the blast to reach discrete points. This time is referred to as time of arrival (TOA). A distance versus time relationship was used to calculate shock front velocity [9]. Static pressure was determined using the Rankine-Hugoniot relation.

This report presents free field pressure data for a cylindrical warhead and is part of an ongoing program to measure blast waves produced from non-spherical high explosives. The focus of the current paper is to compare experimental overpressure from a cylindrical explosive warhead with numerical results for both a cylindrical and a spherical warhead.

The work contained in this report contributes to the Defence Science and Technology Organisation's experimental and theoretical capability to assess blast damage mechanisms of anti ship missile defence weapons. This document is the first of two parts. In this report, the analysis of results is for the free field. In the second report, the analysis is extended to blast / target interaction. An understanding of the lethality of anti ship missile defence weapons is important to be able to provide the Royal Australian Navy with advice relating to weapon procurement and platform vulnerability.

2. Experimental Set-up

Time of arrival measurements and overpressure histories have been recorded for four separate firings, however for convenience all of the results will be dealt with irrespective of the different firings. A photograph of the test arena set-up showing the explosive warhead and the various gauge stands is shown in Figure 1. In each test, a bare cylindrical warhead of Composition B (60 : 40) explosive was placed at a vertical height of 2015 mm from a concrete pad. The nominal diameter, length and mass of the warheads were D = 141 mm, L = 304 mm and Mass = 7.835 kg, respectively.

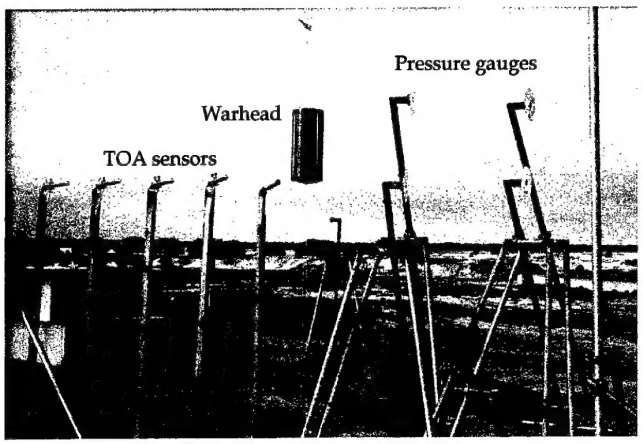

Figure 1. Photograph of the cylindrical warhead and instrumentation.

2.1 Pressure Measurements

For mid and far field blast measurements it is important to mount instrumentation as high as practically possible in order to minimise interference from ground reflections. The majority of pressure gauges and all the time of arrival sensors were placed at the same vertical height of approximately 2000 mm and varying horizontal distances from the warhead. This horizontal distance is the straight-line distance from the vertical centreline of the warhead to the sensor or gauge. Pressure gauges were placed as close to the warhead as possible, which from previous work with a similar explosive warhead [8] was determined to be 1980 mm. Moving the pressure gauges closer to the warhead would have resulted in possible damage to the gauges or erratic results. However a pressure gauge was placed at a nominal 1000 mm vertical height and at a horizontal distance of 1010 mm. This results in the gauge being situated downwards at an angle of 45° from the warhead centre. Due to the cylindrical geometry and the orientation of the warhead, this gauge position will experience lower pressure and exposure to fireball effects than if it had been situated at the 2000 mm vertical height.

Pressure was measured with Endevco (model # 8530B) pressure gauges. These are rated to a maximum pressure limit of 6896kPa (1000 psi). The Endevco gauges employ a silicon diaphragm onto which a four-arm wheatstone bridge has been diffused. Compensation and balancing elements are also included. The gauges were mounted side-on to the direction of the blast wave. Each pressure gauge was mounted inside a machined nylon (Delrin) and O-ring mount, which in turn screwed into the centre of a baffle plate. The nylon mount is used in an attempt to damp high frequency vibration. A baffle plate is shown in Figure 2. The baffle plate is a machined aluminium knife edged disk, which is affixed to the top of a gauge stand. This ensures that minimal aerodynamic interference is encountered in the vicinity of the gauge. The diameter of the knife edged disk was approximately 240 mm.

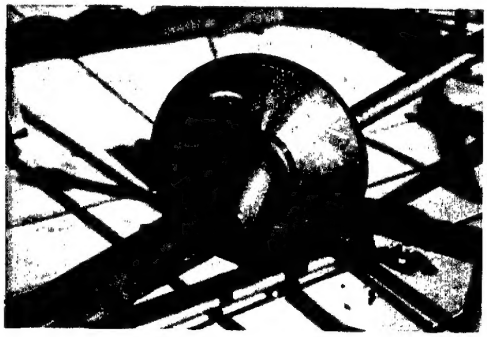

Figure 2. Photograph showing baffle plate used to mount the pressure gauge.

Stands used for mounting pressure gauges must be extremely robust, yet still allow for fine position adjustment. The stands must also be designed to minimise gauge vibrations or "ringing". The stands used for this series of experiments were manufactured from 48 mm O.D. galvanised water pipe which has a nominal wall thickness of 4 mm. They consisted of a pair of forward legs and a longer diagonal piece that acted both as the third leg and the mounting arm for the gauge assembly. These two sections were held together by a commercially available coupling knuckle which allowed for some height adjustment. The array of pressure gauge stands is shown in Figure 3. The stands are designed to provide working heights of 1000 mm or 2000 mm. An additional section can also be added to increase the working height of the 2000 mm gauge stand to 2600 mm. These stands were anchored to the concrete test pad (12 m × 12 m) with a clamp that fitted into Unistrut channels. This type of stand is usually used in an array of up to four or five gauges and these are aligned to minimise shrouding or interference from adjacent gauges.

Figure 3. Pressure gauge stands. The gauge at 1000 mm height is shown in the lower right corner.

Pressure measurements were recorded on Digistar III stand-alone recorders. These feature a programmable digitising rate of up to 5 million samples per second at 12 bit resolution and have up to 4 Mb sample memory. They can be powered by an external 12V supply and have been designed for operation in harsh environments. Measurements from each pressure gauge are recorded on individual Digistar units and are then downloaded onto a laptop computer where the information is subsequently processed.

2.2 Time of Arrival Sensors

The time of arrival sensors were placed at horizontal distances of 915 mm to 3185 mm and a vertical height of 2000 mm. Sensors used in TOA measurements require a rapid response time (< 1μs) and must be physically small so that they do not significantly distort the shock front. Also, there is a need for large numbers of sensors to be used in order to get accurate spatial information of the shock wave. The advantage of this technique is that time of arrival sensors can be placed at very small distances from the explosive. The time of arrival sensors used for these experiments were Dynasen CA-1134 piezoelectric pins. These pins have a 3.175 mm diameter and utilise 0.508 mm thick PZT-5A crystal. These small sensors produce an electrical signal proportional to pressure when impacted by a fast moving object or shock front. This type of piezoelectric pin is normally used for velocity of detonation measurements, where they are in direct contact with the explosive, or for measuring time of arrival of stress waves in solid materials. Therefore, this type of sensor is insensitive to many undesirable stimuli that can excite pressure gauges. For a similar sized warhead to the one used here, it has been determined that these sensors are sensitive enough to measure blast time of arrival at distances of up to 5000 mm. These sensors are considered to be disposable because they are approximately one hundredth of the cost of a pressure gauge.

The pin sensors were mounted in the tip of a solid aluminium cone that was attached to a 32 mm diameter aluminium pipe that was approximately 400 mm long, as shown in Figure 4. This assembly was affixed to a 2000 mm high stand that was manufactured from similar material to the pressure gauge stands as shown in Figure 1. The TOA stand consisted of a slightly angled upright pipe that was attached to a steel base plate. Since the height was fixed at 2000 mm, the stand was simply aimed at the warhead centreline and bolted into position in the Unistrut channel. Some horizontal adjustment was possible by moving the aluminium pipe in and out.

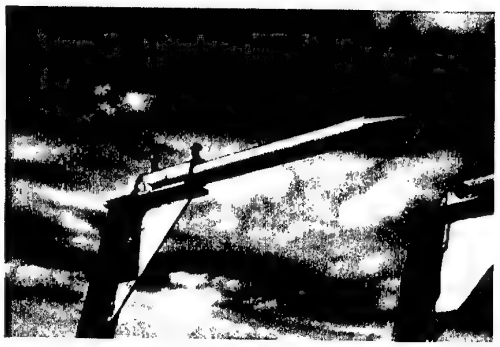

Figure 4. Time of arrival sensor.

Although these sensors can easily be multiplexed, it was decided not to in order to ensure reliability and simplicity. Each sensor was directly connected to a single channel with no added amplification or conditioning of the output signals. Four sensors were used for each firing and their outputs were sent to individual channels of a 4 channel Tektronix TDS 544A digital storage oscilloscope. Data from this was transferred onto a laptop computer using GPIB software.

2.3 Photo instrumentation

Photo instrumentation activities included a Hycam rotating prism camera which was used to capture the shock wave travelling across a zebraboard background. As a backup for this, a NAC-E10 rotating prism camera was also used to provide another film, which could be used to test for correct exposures, and as a primary camera in the event of a Hycam failure. A Locam camera was used to provide a high speed colour documentary of each explosive event. A Minolta 35 mm camera was also used in sequencing mode to give still images of each event.

Figure 5 shows the arena set-up with the zebraboard. The zebraboard was 4.8m wide and 1.2m high. Situated along the bottom and top of the zebraboard were fluorescent lamp reflectors which were used to hold slow peak - long duration flash bulbs. The zebraboard was made from steel tubing, with a steel wire mesh to hold 100 mm wide x 1 mm thick aluminium strips (zebra stripes) running at 45 degrees. Setting the zebra stripes at 45 degrees improves the shock wave signature on the film.

The increase in density caused by the blast wave, increases the refractive index of the air. It is this change of refractive index at the shock wave edge, which visually distorts the image of the background, subsequently allowing the shock wave to be recorded photographically, as shown in Figure 6. The position of the shock wave and time from detonation can be measured from the film and used to calculate velocity.

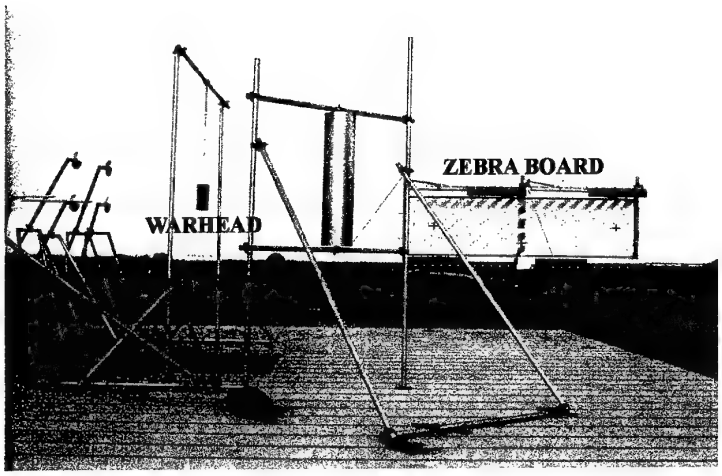

Figure 5. Arena set-up showing the zebraboard.

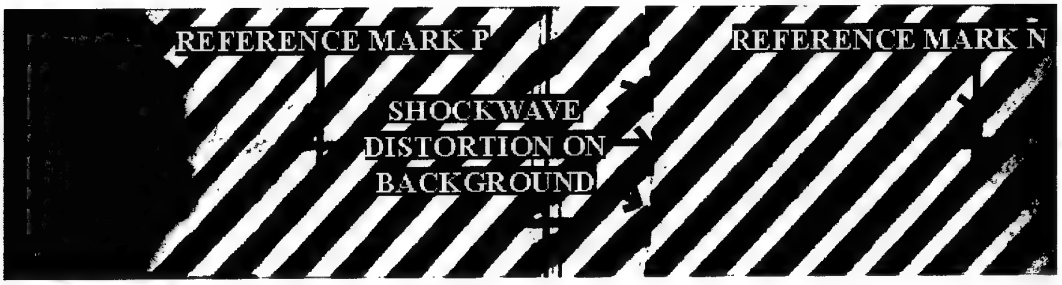

Figure 6. Photograph of the zebraboard showing the visual distortion created by shock wave.

Both the Hycam and the NAC-E10 were fitted with half height heads, which better suit the field of view required when using the zebraboard background. The field of view of each camera covered the entire width of the background. This also allowed a slower framing rate to be set, i.e. half that of a full height head, thus saving wear on the camera. The "event out" signal from the Hycam camera was used to trigger the firing of the explosive warhead. The camera takes approximately 1 second to reach the required speed, and can record for approximately 1.4 seconds at speed, using a 100 ft reel of film. Both cameras were run at a nominal framing rate of 3000 frames/second, effectively 6000 half frames/second. Mirrors were used to film the zebraboard from within a protective structure called a splinter proof, in order to protect the cameras from the blast. The splinter proof was positioned 43m from the warhead. The film used was 16 mm black and white Kodak 7278 Tri-X Reversal. The Locam camera was set to run at 500 frames/second. This camera recorded an overall view of the test arena. This imaging provided a high speed record of each event which was later transferred to video (Betacam). The video from event 4 was also converted into an AVI (audio visual interlaced) file, and digital stills.

There are two components to the analysis of the 16 mm film in providing velocity data of the shock wave. The first component is to derive timing information from the film rebate, using an event mark which has been exposed on the film, and timing marks which had been set at 1000 Hz. The 16 mm film is placed on a light box and several timing marks are measured to provide the camera's running speed, as shown in Figure 7. The distance between 6 timing marks is measured in millimetres, and averaged. The average distance between the 6 timing marks is then divided by the height of a 16 mm frame (7.605 mm). This value provides us with the number of frames that have been recorded per millisecond. The event mark (also recorded on the film rebate) as seen in Figure 8, is used to determine the exact position of T_0 (time of detonator initiation) on the film. For the Hycam camera, the T_0 image will lead the timing light signal by 5 frames. As the film rebate is visible on the film analyser, the operator can reset the film frame counter to zero by viewing the event mark next to a frame, and going backward 5 frames. Any measurements taken are then allocated the relevant frame number, and timing information.

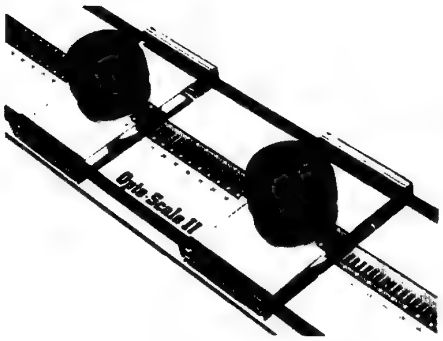

Figure 7. Opto Scale used to measure timing Marks.

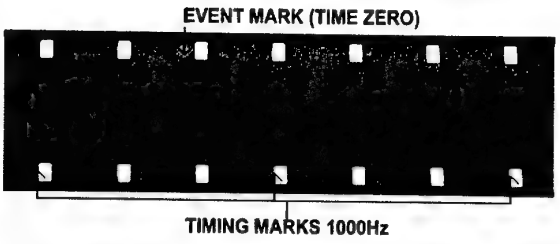

Figure 8.Event Mark and Timing Marks.

The second component of the analysis is to calculate the shock wave position from the centre of the warhead. The 16 mm film is projected onto a frosted glass screen in a NAC 160F Motion Picture Analyser, as shown in Figure 9. The operator uses a cursor as illustrated in Figure 10, to measure X and Y coordinates from two reference points, and the outside edge of the shock wave. The NAC analyser provides data points in generic NAC units, which the operator converts to millimetres by using the trial site survey data.

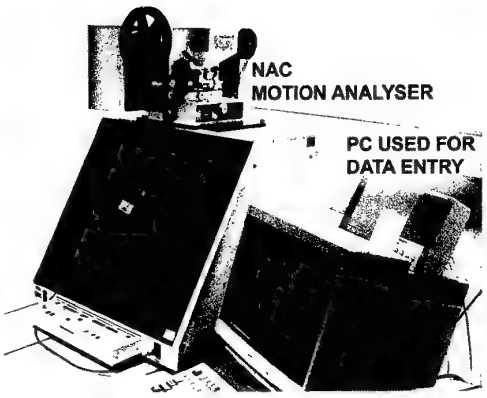

Figure 9. NAC 160F Motion Picture Analyser.

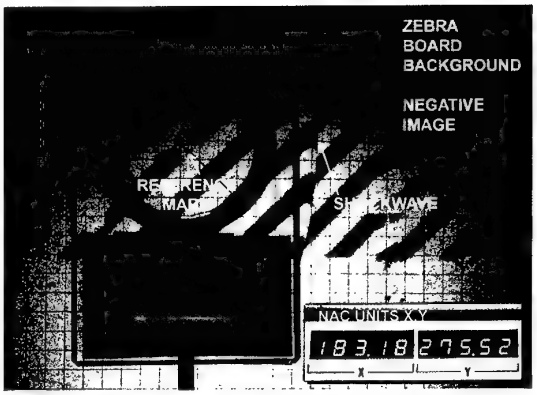

Figure 10. Gathering X and Y co-ordinates of reference marks and shock wave position.

Figure 11 shows how a typical frame would be analysed. For each frame being analysed, three coordinates are measured, they are reference mark 1 (P) X_1Y_1, reference mark 2 (N) X_2Y_2, and the shock front position (Z) X_3Y_3. Each position is measured three times and then the average value of the three is used to reduce human error. Whilst these values are in NAC units, the following equations are used to calculate the position of the shock front (Z) relative to the warhead position (C) X_4Y_4 using the NAC analysis data and the survey data, whilst correcting any film jitter or camera movement.

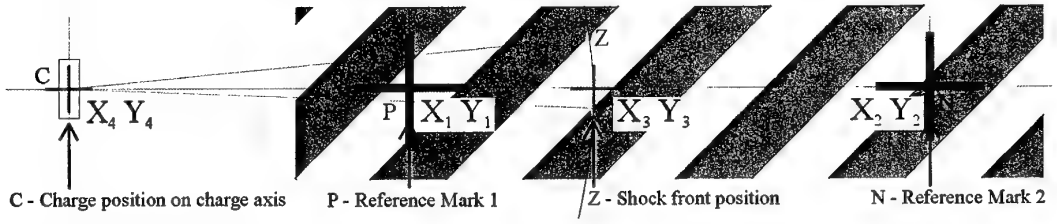

Figure 11. Warhead position relative to shock front position, and reference points P and N [10].

The X,Y coordinates measured in Figure 11, are used to determine the distance between P and N in NAC units, using Equation 1. The distance in NAC units can then be compared to the distance in millimetres from the survey data, and a scale factor from NAC units to millimetres can be calculated.

$$PN = \sqrt{(X_2 - X_1)^2 + (Y_2 - Y_1)^2} \quad (1)$$

The gradient of the line between P and N is calculated using Equation 2. Checking the slope of P and N for each image, allows a correct warhead position to be established, even if the film jitters between frames in the analysis projector.

$$C3 = \frac{Y_2 - Y_1}{X_2 - X_1} \tag{2}$$

By using the scale factor calculated from Equation 1, the distance CP from the site survey data, is converted from millimetres to NAC Units. The NAC value of X and Y at position C is then calculated using Equation 3 (based on position P) or Equation 4 (based on position N).

$$X_4 = X_1 - \frac{CP}{\sqrt{1 - C_3^{\,2}}} \text{ and } Y_4 = Y_1 - (X_1 - X_4) \times C_3 \tag{3}$$

$$X_4 = X_2 - \frac{CN}{\sqrt{1 - C_3^{\,2}}} \text{ and } Y_4 = Y_2 - (X_2 - X_4) \times C_3 \tag{4}$$

The result from Equation 3 and Equation 4 should be the same. The option of using either reference mark is available so that if the shock wave distortion on the background, blast products, or target debris were to obscure one of the reference marks, the warhead position relative to the shock wave position can still be calculated.

Equation 5 calculates the distance of CZ in NAC units. The scale factor calculated from Equation 1, is then used to convert the distance of CZ from NAC units to millimetres.

$$CZ = \sqrt{(X_3 - X_4)^2 + (Y_3 - Y_4)^2} \tag{5}$$

The calculations done thus far provide the position of the shock wave on the zebraboard background. The zebraboard was situated back away from the actual shock wave so that it would not be damaged, nor interfere with the shock wave. Figure 12 illustrates the geometry of the trial site.

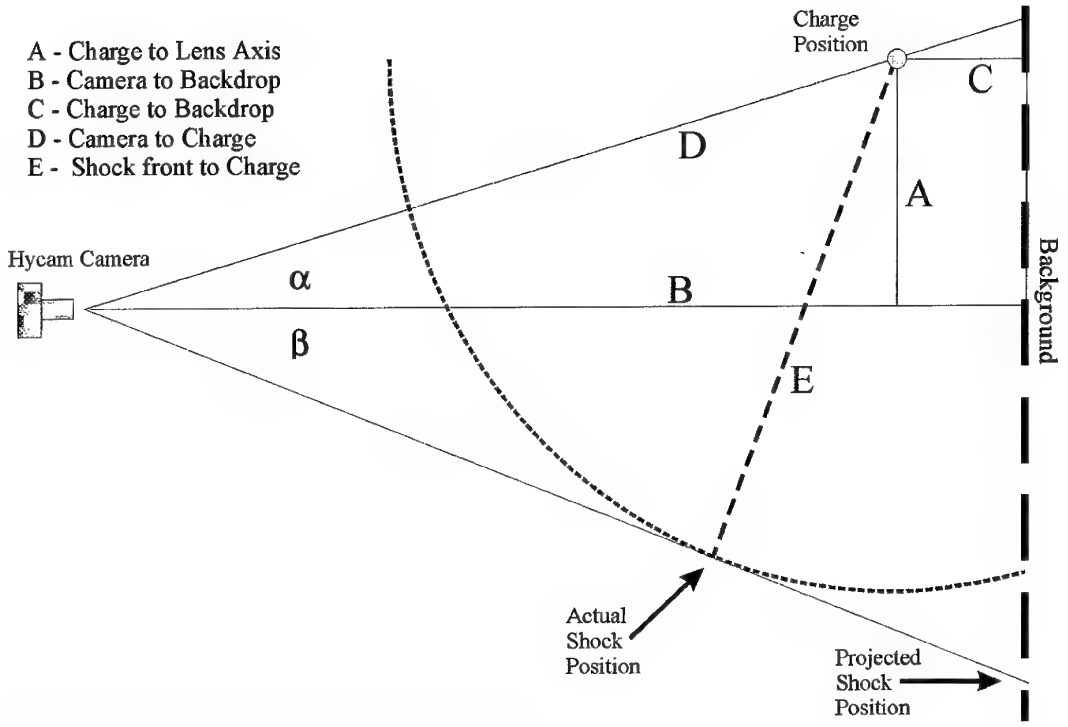

Figure 12. Schematic Geometry of the trial site [10].

Equation 6 is used to calculate the actual shock wave position. An imaginary line running from the camera, to the edge of the shock wave, and to the projected shock position, forms a tangent to the shock wave, and therefore the value of $\alpha+\beta$ degrees, and the length of D, can be used to find the length of E which is the actual shock wave position from the centre of the warhead.

$$E = D \sin(\alpha+\beta) \tag{6}$$

3. Numerical Model

A computational fluid dynamics analysis was conducted using IFSAS (Integrated Fluid Structure Analysis Software). In the numerical model, the flow is assumed to be two-dimensional, compressible and inviscid. Free Slip conditions are applied at all solid boundaries. The code uses an explicit second order Lax-Wendroff scheme with 6th order Flux Corrected Transport. Two cases have been modelled. The first case involves modelling the blast from a bare cylindrical warhead and is intended to be a direct comparison with the experimental tests. The second case is based on a bare spherical explosive warhead and is included here to illustrate the different blast profiles of cylindrical and spherical warheads. It should be stated, that the computational analysis here is not intended to be a predictive tool. Rather, the aim of the numerical work is to provide a complete two-dimensional representation of the blast in the free field. The complicated physics of the explosive detonation is not included in the model.

Therefore, the validity of the model deteriorates in the near field. However, the model is relatively accurate in the far field, as shown in Section 4.

3.1 Initial Conditions

The blast effect of the detonation is modelled by setting an initial region of high pressure and high temperature. The initial conditions of this high pressure, high temperature region have been determined using the "balloon" analogue of Ritzel and Matthews [11]. The methodology described by Ritzel and Matthews is based on the work of Brode [12]. The initial high pressure, high temperature region is referred to as a balloon of nil confinement. The total blast energy of a pressurised balloon containing an ideal gas is given by Equation 7,

$$E = \frac{V(P - P_o)}{\gamma - 1} \tag{7}$$

where E is the available blast energy of the warhead, P is the initial pressure, P_o is the ambient pressure, V is the volume of the balloon and γ is the ratio of specific heats for the gas in the balloon. These parameters may be adjusted in order to "tune" the numerical results with observations from experiments. The shape of the initial high pressure region should have the same aspect ratio as the explosive. In this investigation, the available blast energy for Composition B is assumed to be 5.117 MJ/kg [8]. For the current series of tests, the average mass of the Composition B high explosive is 7.835 kg. For the cylindrical warhead, the length and diameter of the warhead are L=304 mm and D=141 mm, respectively. Therefore, the total available blast energy is $E=4.00925\times10^7$ J and the initial cylindrical high pressure region must have a length to diameter ratio of approximately L/D=2. The balloon dimensions were set at L=720 mm and D=360 mm, this is in agreement with Wildegger-Gaissmaier et al. [8], where a similar sized warhead was modelled using the balloon analogue. The gas in the balloon was set to be Helium, $\gamma=1.66$. Helium was chosen rather than air because less energy is expended in accelerating Helium during the initial expansion of the balloon [11]. Using Helium to pressurise the balloon has been determined to produce a blast profile close to that created by a high explosive detonation [11]. A summary of the balloon parameters is given in Table 1. Using Equation 7, the pressure of the balloon, P, is determined to be 3.6116×10^8 Pa. The temperature is set at 3000 K in agreement with Wildegger-Gaissmaier et al. [8]. The same balloon parameters were used for the spherical warhead, with the exception that the initial shape of the balloon was spherical with a radius of 260 mm.

Table 1. Initial conditions for the numerical model of the cylindrical explosive warhead.

Diameter	D	360 mm
Length	L	720 mm
Blast Energy	E	$E=4.00925\times10^7$ J
Specific Heat Ratio	γ	1.66
Ambient Pressure	P_o	1.01325×10^5 Pa
Ambient Temperature	T_o	298 K
Balloon Pressure	P	3.6116×10^8 Pa
Balloon Temperature	T	3000 K
Balloon Density	ρ_o	57.93 kg/m^3

3.2 Afterburn Energy

The chemical formula for Composition B shows that it is 43% oxygen deficient for combustion [13]. This means that approximately 40% of the total potential energy of the explosive is released as post detonation energy, referred to as afterburn. Wildegger-Gaissmaier et al. [8] investigated the effects of afterburn and concluded, for a warhead of the size used here, that 3.41MJ/kg should be released into the balloon gas as constant after-burn energy. Since 4.25 kg of Helium was used to create the high pressure balloon, a total of 14.5MJ of afterburn energy was released. In accordance with Wildegger-Gaissmaier et al. [8], this energy was released over 30 milliseconds.

3.3 Grid Set-up

In the experiments, the warhead was positioned at a vertical height of 2015 mm. Due to axi-symmetry only half of the warhead and free field needs to be modelled computationally as shown in Figure 13. A symmetry boundary is located at X=0, and a flow-through boundary at X=6000 mm and Y=4000 mm. The ground is accounted for with a solid boundary at Y=0 with slip velocity condition in the X direction. Static overpressure histories were output at the locations shown in Figure 13. The horizontal (X) and vertical (Y) coordinates of these points is given in Table 2.

The domain shown in Figure 13 was discretised using cells of 20 mm × 20 mm, 15 mm × 15 mm, and 10 mm × 10 mm. The static pressure histories at the points shown in Figure 13 showed convergence for a cell size of 10 mm × 10 mm. Therefore, the numerical results presented in this paper were generated with a grid resolution of 10 mm × 10 mm.

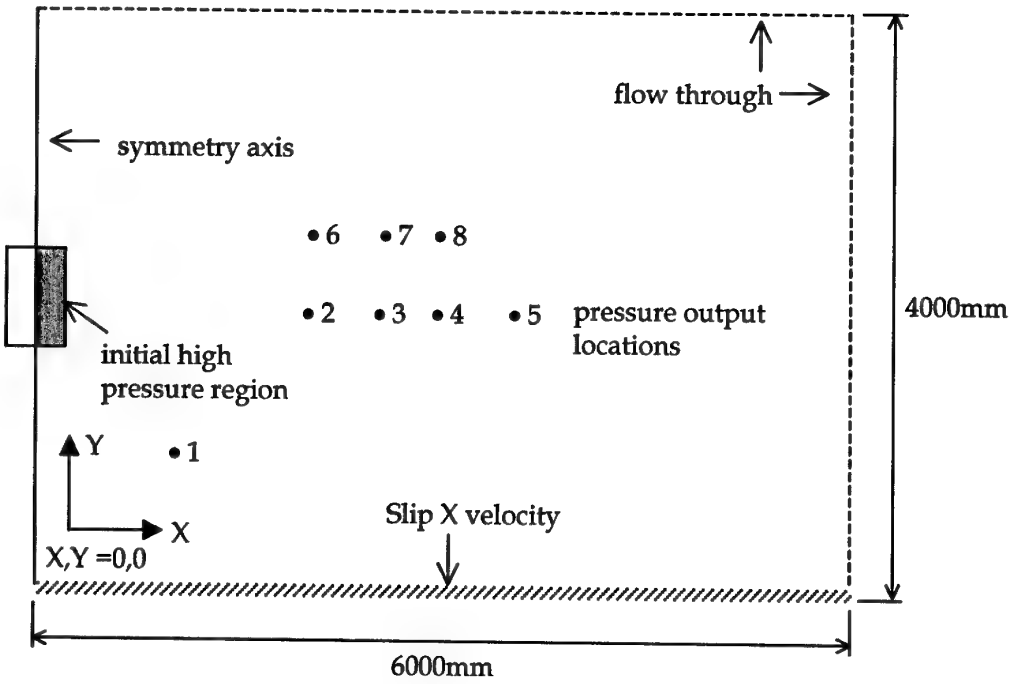

Figure 13. Schematic diagram of numerical model for the cylindrical warhead.

Table 2. Output Locations for Static Overpressure.

Pressure output location	X coordinate	Y coordinate
1	1010	1000
2	1980	2010
3	2520	2000
4	2950	2040
5	3550	2000
6	2010	2610
7	2560	2600
8	2960	2590

4. Results and Discussion

In the following discussion, results recorded during the experiments will be compared with results generated numerically. The numerical method is not predictive and attempts have been made to match the numerical results with the measurements from the experiments. The errors associated with the experimental results have not been quantified. Rather, the approach adopted here is to use multiple techniques to determine the same parameter. For example, overpressure is measured directly with pressure gauges and is also determined from time of arrival data. The discussion of the results has been grouped into four sections comprising, time of arrival, overpressure histories, blast profile plots and fireball.

4.1 Time of Arrival

The time of arrival data recorded with sensors is presented in Table 3. All of the time of arrival sensors were placed at 2000 mm height, which corresponds to the horizontal centreline of the warhead. The distance, X, in Table 3 is the horizontal distance from the vertical warhead centreline to the time of arrival probe. Time of arrival of 16.532ms was also recorded with the PCB pressure gauge located at 9995 mm. Only one result from this gauge was obtained during the four firings. The peak pressure could not be given because the recorded pressure level was higher than the anticipated maximum that was preset on the Digistar recorder. Therefore, only time of arrival information was obtained. Time of arrival data was also determined from the zebraboard images. For one of the events, the shock wave travelling across the zebraboard is shown in Figure 14.

Table 3. Time of arrival data from sensors.

X (mm)	Time (ms)
915	0.3842
1330	0.5211
1360	0.5634
1751	0.7291
1775	0.7739
1885	0.7866
1850	0.8840
2235	1.0203
2240	1.084
2300	1.100
2305	1.194
2720	1.442
2735	1.485
2745	1.588
3165	1.929
3185	2.061

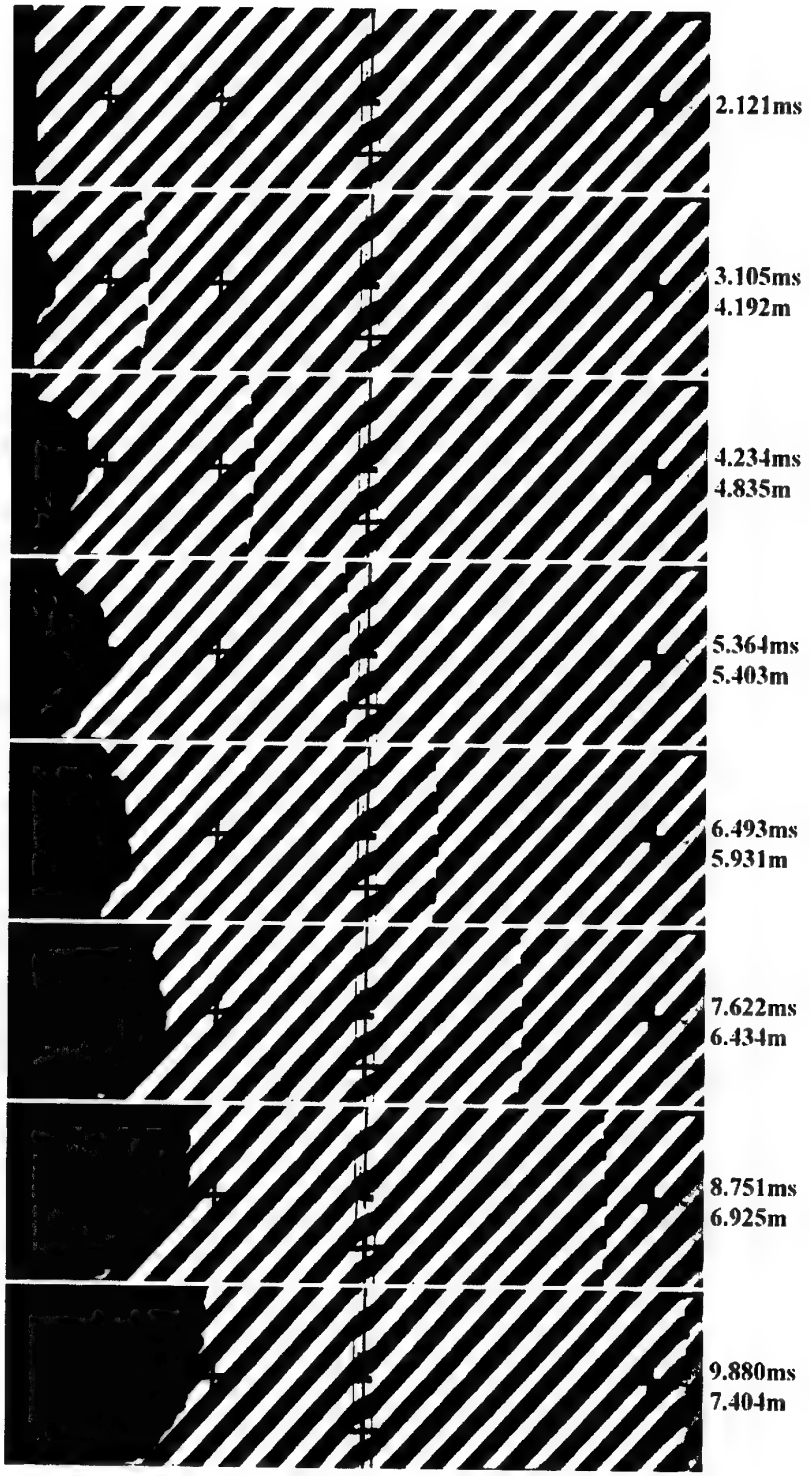

Figure 14. Images of the shock wave distortion on the zebraboard.

The time of arrival data obtained from the zebraboard over two independent events is given in Table 4.

Table 4. Time of arrival data from zebraboard in two separate events.

Event 1		Event 2	
X (mm)	Time (ms)	X (mm)	Time (ms)
3576	2.322	3600	2.258
3678	2.459	3712	2.399
3780	2.595	3818	2.541
3829	2.732	3865	2.682
3973	2.868	4009	2.823
4061	3.005	4106	2.964
4151	3.141	4192	3.105
4244	3.278	4284	3.246
4326	3.415	4365	3.388
4408	3.551	4448	3.529
4488	3.688	4531	3.670
4568	3.824	4609	3.811
4643	3.961	4687	3.952
4718	4.098	4767	4.093
4795	4.234	4835	4.234
4864	4.371	4912	4.376
4938	4.507	4984	4.517
5008	4.644	5052	4.658
5078	4.78	5125	4.799
5152	4.917	5196	4.940
5218	5.054	5262	5.081
5286	5.19	5336	5.222
5354	5.327	5403	5.364
5419	5.463	5471	5.505
5486	5.6	5536	5.646
5552	5.737	5603	5.787
5617	5.873	5668	5.928
5680	6.01	5732	6.069
5743	6.146	5801	6.210
5805	6.283	5866	6.352
5874	6.419	5931	6.493
5933	6.556	5997	6.634
5994	6.693	6057	6.775
6057	6.829	6119	6.916
6121	6.966	6182	7.057

Table 4 continued. Time of arrival data from zebraboard in two separate events.

Event 1		Event 2	
X (mm)	Time (ms)	X (mm)	Time (ms)
6181	7.102	6246	7.198
6240	7.239	6307	7.340
6300	7.376	6372	7.481
6364	7.512	6434	7.622
6425	7.649	6496	7.763
6484	7.785	6558	7.904
6544	7.922	6628	8.045
6606	8.058	6680	8.187
6661	8.195	6740	8.328
6723	8.332	6801	8.469
6785	8.468	6862	8.610
6840	8.605	6925	8.751
6900	8.741	6985	8.892
6958	8.878	7044	9.033
7015	9.015	7103	9.175
7076	9.151	7164	9.316
7130	9.288	7207	9.457
7188	9.424	7280	9.598
7235	9.561	7343	9.739
7301	9.697	7404	9.880
7359	9.834	7464	10.021
7420	9.971		
7479	10.107		

The time of arrival data from the sensors, zebraboard and Pitot static pressure gauge is plotted in Figure 15, with a fitted curve of the form:

$$X = a_{60} + ct + a_{62}\ln(t) + \frac{a_{63}}{t} \qquad (8)$$

where X is the distance from the warhead and the values of the constants, a_{60}, a_{62} and a_{63} are 8.6354, 0.9781 and -2.7729×10^{-5}, respectively. The remaining parameters in Equation 8, are the speed of sound, c=340m/s, and time, t.

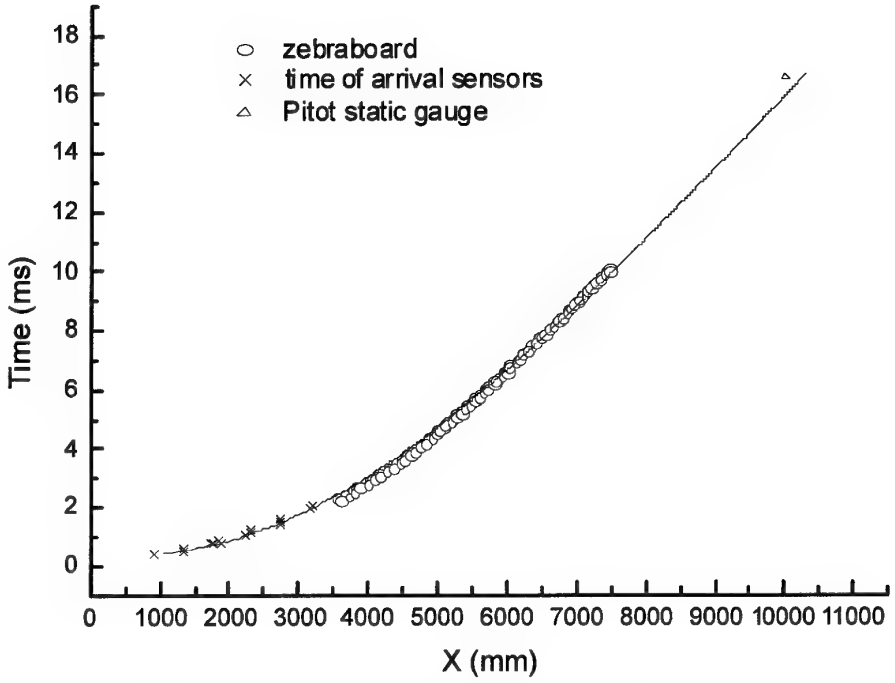

Figure 15. Shock front time of arrival measured with sensors, zebraboard and Pitot static pressure gauge.

The fitted curve in Figure 15 accurately represents the trend of the data. Equation 8 was differentiated to determine velocity of the blast wave. This enables Mach number to be calculated as a function of distance [9]. By assuming the shock to behave as an ideal gas, the Rankine-Hugoniot relation can be used to give Equation 9, where P is the shock wave pressure, P_o is ambient pressure, γ the ratio of specific heats and M is Mach number.

$$\frac{P}{P_o} = 1 + \frac{2\gamma}{1+\gamma}\left[M^2 - 1\right] \tag{9}$$

Overpressure ($P-P_o$), as a function of distance from the warhead is shown in Figure 16. Also shown in Figure 16 are overpressures measured during the experiments. Future work will employ time of arrival measurements to determine overpressures at distances of a few millimetres from the warhead.

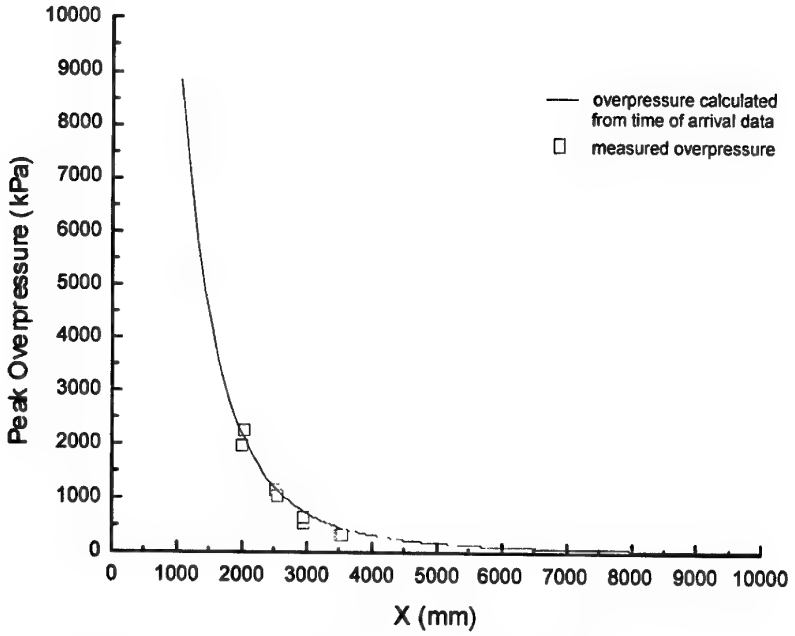

Figure 16. Peak overpressure versus distance from the warhead.

4.2 Overpressure Histories

Typical blast overpressure histories from various pressure gauges are shown in Figure 17 to Figure 20. Also shown for comparison in each of these figures are the numerical results for spherical and cylindrical warheads. As stated in Section 2.1, the pressure gauges were positioned at various horizontal distances (1010 mm < X < 3550 mm) and at three different heights. These gauges were positioned such that their heights were nominally 1000 mm, 2000 mm and 2600 mm. The entire set of pressure histories recorded during the trial is given in Appendix A.

Figure 17(a) shows the results for a gauge located at a horizontal distance of X=1010 mm and a vertical height of Y=1000 mm. It can be seen that there are significant differences between the numerical results and the experimental overpressure record. Figure 17(a) illustrates the limitation of the numerical model in the near field. The magnitude of the numerical overpressure for the spherical warhead was 2727 kPa and as expected, this is higher than the overpressure for the cylindrical warhead, which was 1924 kPa. This is due to the non-uniform blast of the cylindrical warhead. The magnitude of the experimental measurement was 1192 kPa and this is considerably less than the numerical result. It should also be noted that, in the experiment, the peak overpressure occurs later than numerical results. Clearly, a different approach is required to model blast in the near field.

Figure 17(b), shows the results from a gauge situated at a horizontal distance of X = 1980 mm and a height of Y = 2010 mm. The agreement is better than in Figure

17(a). The experimental peak overpressure of 1992 kPa is higher than the numerical result of approximately 1630 kPa for a cylindrical warhead and 1053 kPa for a spherical warhead. Although there are differences between the results from the experiments and the numerical values, the trend of the numerical results is reasonably accurate. The numerical results show that the overpressure from a cylindrical warhead can be higher than that from a spherical warhead. This phenomenon was also observed by Swisdak [14]. Swisdak [14] found that the peak overpressure from cylindrical warheads with L/D=2 was approximately 1.6 times greater than the blast caused by spherical warheads.

It would have been possible to achieve closer agreement with experimental results in Figure 17(b) by increasing the initial balloon pressure, however, this would have resulted in greater differences in other regions of the flow field. This is evident in Figure 18(a), which shows the experimental and predicted overpressures at a similar horizontal distance from the warhead but at a height of 2600 mm instead of 2000 mm. As can be seen, reasonable agreement has been achieved. The predicted overpressure for the cylindrical case was 1269 kPa compared to the measured overpressure which was 1066 kPa. However, if the initial balloon pressure in the model was increased to correct for the variations seen at the 2000 mm height, the calculated overpressure would have been even higher at the 2600 mm height.

Figure 18(b), shows overpressure histories at a horizontal distance of X = 2520 mm and vertical height of Y=2000 mm. The peak experimental overpressure was 1160 kPa while the calculated level for the cylindrical case was approximately 812 kPa. For the spherical case the predicted level is even less at 591 kPa. Obviously, this difference has serious implications when determining the resultant blast damage effects. Further work is required to model the blast overpressures in the near field region.

Results from a gauge positioned at X=2560 mm and height of Y=2600 mm, are shown in Figure 19(a). This location can now be considered as the mid field region. Figure 19(a) shows a relatively good agreement between the experimental overpressure of 724 kPa and the magnitude of the calculated overpressure for the cylindrical warhead of 663 kPa. Figure 19(b) shows results from a position of X=2950 mm and a height of Y=2040 mm. There is reasonable agreement between the measured experimental overpressure and the calculated overpressure for the cylindrical warhead. The measured overpressure of 675 kPa was once again higher than the calculated result for the cylindrical case, which was 496 kPa. As expected, the calculated result for the spherical warhead of 384 kPa was lower than the overpressure from the cylindrical warhead.

Figure 20(a) shows results for a gauge positioned in the mid to far field, at a distance of X=2960 mm and a height of Y=2590 mm. The measured overpressure was 594 kPa which is higher than the numerical result of 453 kPa for the cylindrical warhead. Once again, the result predicted for spherical warhead was lower at 362 kPa. Figure 20(b) shows the results for the gauge positioned in the far field, where X=3550 mm and Y=2000 mm. At this distance, the measured and the calculated result for the cylindrical

warhead show good agreement. The magnitude of the measured overpressure was 338 kPa compared to 296 kPa for the cylindrical warhead. Furthermore, the difference in peak overpressure between the cylindrical warhead (296 kPa) and the spherical warhead (242 kPa) is also relatively small.

The results shown in Figure 17 to Figure 20 suggest that the differences between the cylindrical and sperical warheads are more apparent in the near field and that the respective blast overpressure levels are comparable in the far field. Future work will involve further analysis of the numerical results along the vertical centre line to determine if the same trends are apparent.

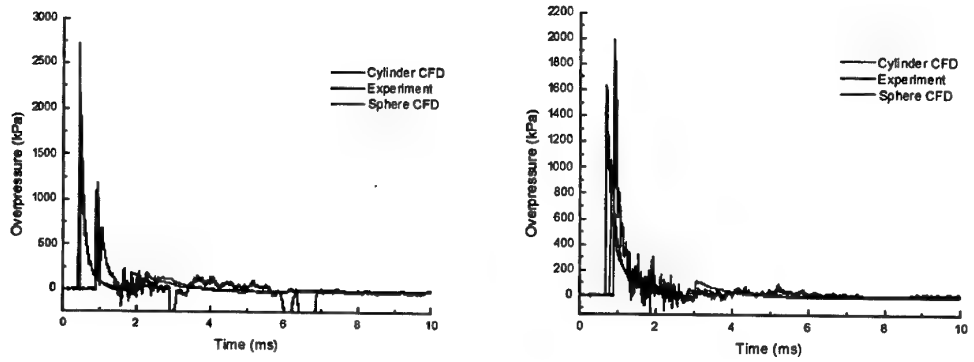

Figure 17. Experimental and computational overpressure histories at (a) X=1010 mm and Y=1000 mm and (b) X=1980 mm and Y=2010 mm.

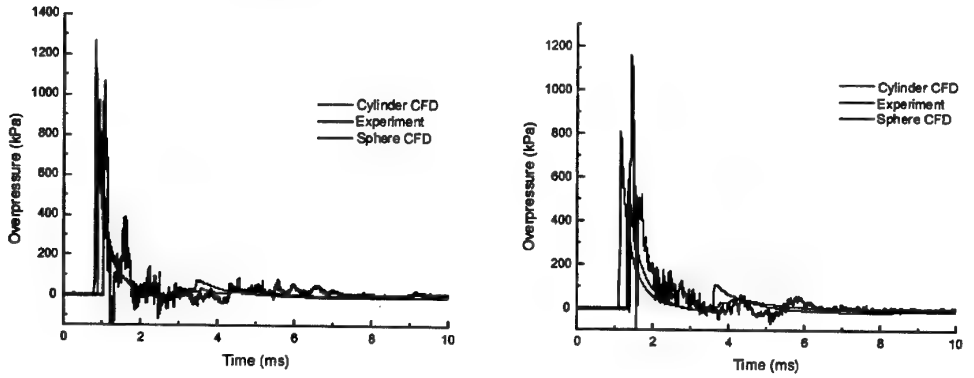

Figure 18. Experimental and computational overpressure histories at (a) X=2010 mm and Y=2610 mm and (b) X=2520 mm and Y=2000 mm.

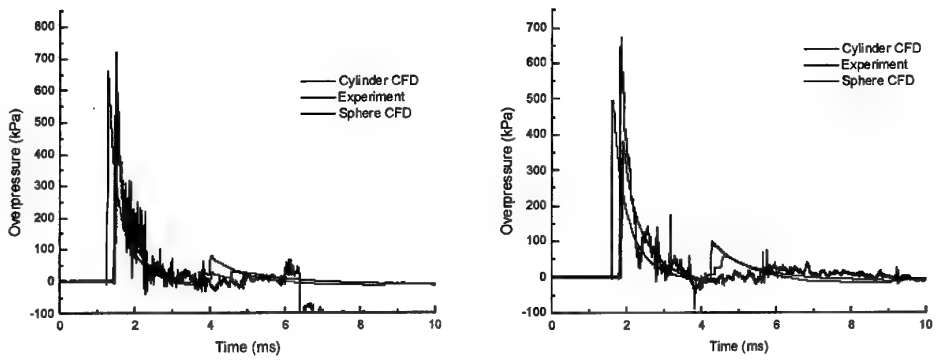

Figure 19. Experimental and computational overpressure histories at (a) X=2560 mm and Y=2600 mm and (b) X=2950 mm and Y=2040 mm.

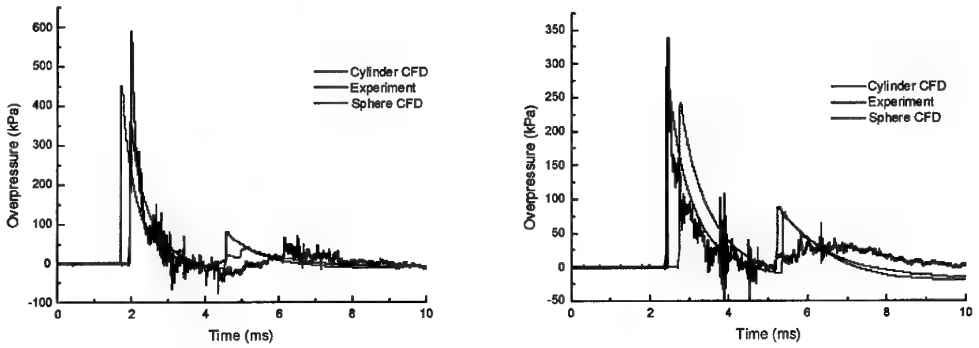

Figure 20. Experimental and computational overpressure histories at (a) X=2960 mm and Y=2590 mm and (b) X=3550 mm and Y=2000 mm.

4.3 Blast Profiles

The numerical model was used to generate contour plots of static pressure shown in Figure 21 and Figure 22 for the cylindrical and spherical warheads, respectively. Each frame represents the static pressure profile at the time shown at the top of the frame. Overpressure may be calculated by subtracting the ambient pressure of 101.325 kPa.

In Figure 21(a) and Figure 22(a), the initial balloon for the cylindrical and spherical warheads are shown. Figure 21(b) and Figure 22(b) show pressure contour plots at 1 millisecond. In both figures, the blast wave has travelled a relatively short distance from the warhead and is classified as being in the near field. The accuracy of the numerical model is limited in the near field, however, these contour plots may still be useful for a qualitative comparison between blast from cylindrical and spherical

warheads. In Figure 21(b), the high pressure gas in the balloon has expanded to a horizontal distance of over 2000 mm. The initial blast wave has an obvious non-uniform shape. The blast is more focused at the horizontal centreline of the warhead at Y=2015 mm. A reflection of the blast is visible at the lower left corner of the frame. The spherical case shown in Figure 22(b), shows a uniform blast profile, also with a ground reflection visible at the lower left corner.

Figure 21(c) through to Figure 21(f) show the development of the blast wave in 1 millisecond intervals for the cylindrical case. The reflection of the blast wave that was visible at 1 millisecond develops into a Mach stem and is clearly visible after five milliseconds as the highest pressure region in Figure 21(f). An important feature to note here is that the static pressure is considerably higher in the region of the mach stem compared with the rest of the blast wave in Figure 21(f). The corresponding frames for the spherical case in Figure 22(c) through to Figure 22(f) show a similar trend to the cylindrical case. A Mach stem is also clearly shown in Figure 22(f).

In Figure 21(f) and Figure 22(f) for the cylindrical and spherical warheads, respectively, the blast waves have travelled a significant distance and can be classified as being in the far field. The differences between the blast waves are less apparent in these figures.

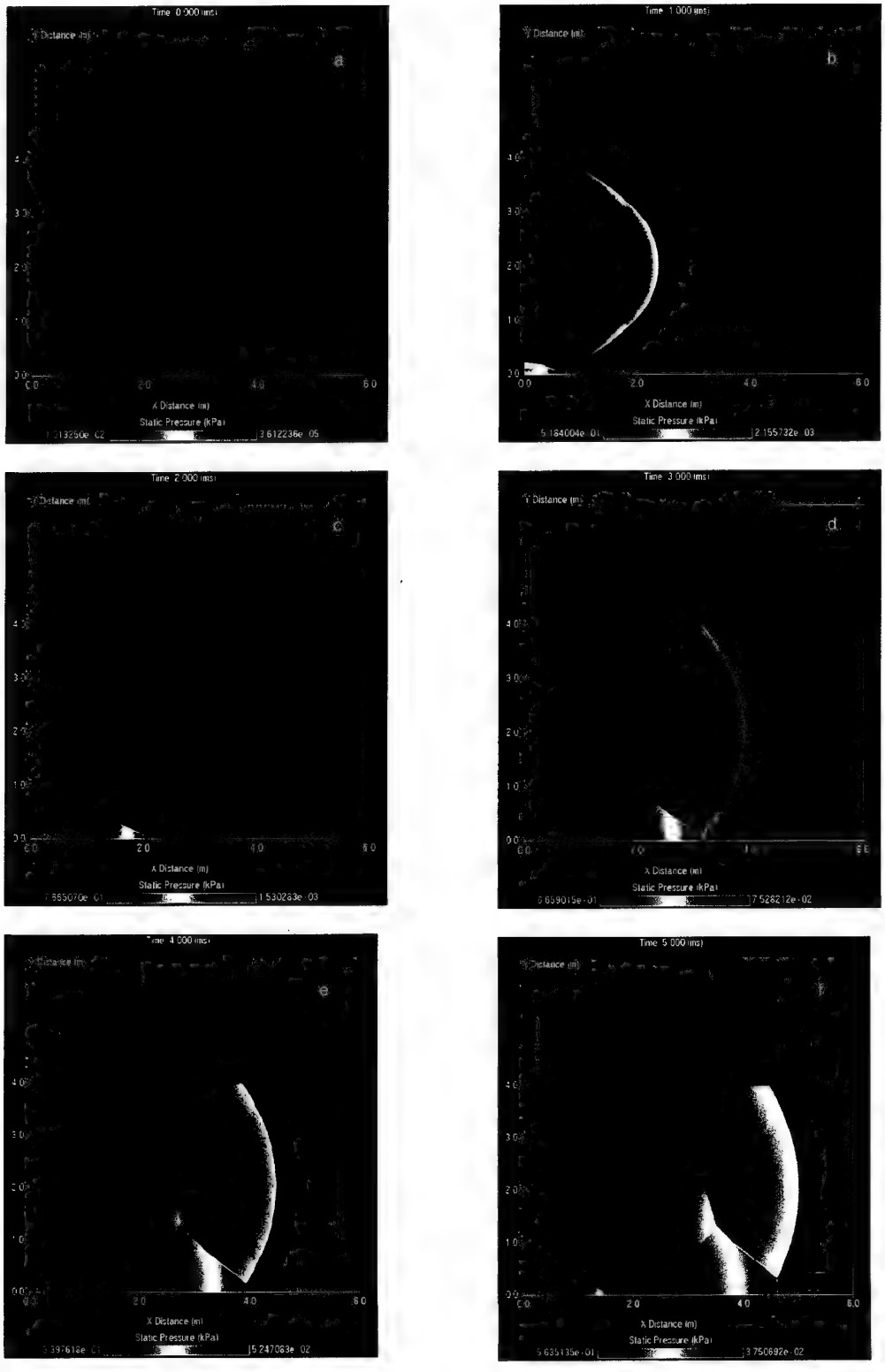

Figure 21. Static pressure contour plots for the cylindrical warhead.

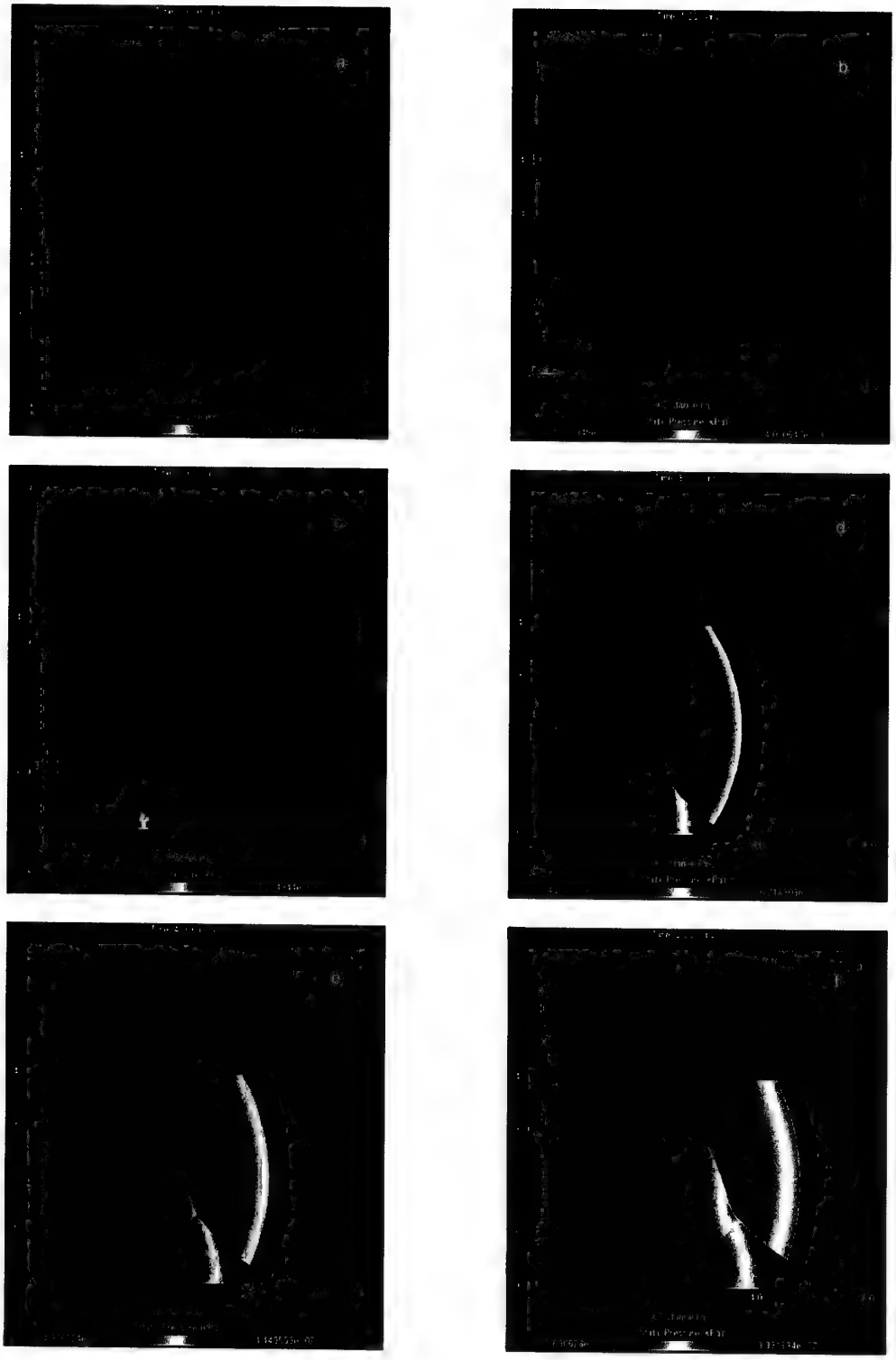

Figure 22. Static pressure contour plots for the spherical warhead.

4.4 Fireball

After the detonation of a high explosive like Composition B, the detonation products continue to expand into the free air. The expansion of the detonation products causes mixing with the oxygen in air and allows the combustible components of the detonation products to burn. This is known as the fireball [15].

A series of fireball images recorded with the Locam camera is shown in Figure 23. Figure 23 shows that the fireball is non-spherical and has a significant horizontal component. The images in Figure 23 can be compared with contour plots from the numerical model. As discussed in Section 3, the numerical model does not simulate the detonation of the high explosive. However, the numerical results can be used to provide a qualitative analysis of fireball growth [8]. By assuming that the fireball and detonation products do not mix with the ambient gas, a contour plot of ratio of specific heats shows how the gas in the initial high pressure "balloon" expands. In the model, the explosion source is a high pressure helium balloon. Helium has a specific heat ratio of γ =1.667. The ambient gas used was air with a specific heat ratio of γ =1.4. Figure 24 shows contour plots of specific heat ratio for the cylindrical warhead. The contour plots are for 1 millisecond intervals from 0 to 5 milliseconds. At Time=0, Figure 24 shows the initial shape of the high pressure balloon. After 1 millisecond, the gas in the high pressure balloon has expanded into a shape representing a cross with significant vertical and horizontal components. This highlights the non-uniform expansion of the cylindrical balloon as observed in Section 4.3. Figure 24, shows the gas in the balloon continues to expand in the shape of a cross and after 5 milliseconds has a similar shape to that shown in Figure 23, though the time increments of Figure 23 and Figure 24, are not synchronised.

For comparison purposes, Figure 25 shows contour plots of specific heat ratio for a spherical warhead, at 1 millisecond intervals. At time zero, the spherical shape of the initial high pressure balloon can be seen. At 1 millisecond this high pressure gas has expanded and approximately retained its spherical shape. There is also the formation of multiple "jets". The origin of these jets is unclear. Further investigation is required to determine if the presence of the jets occurs in reality or whether they are a characteristic of the numerical procedure.

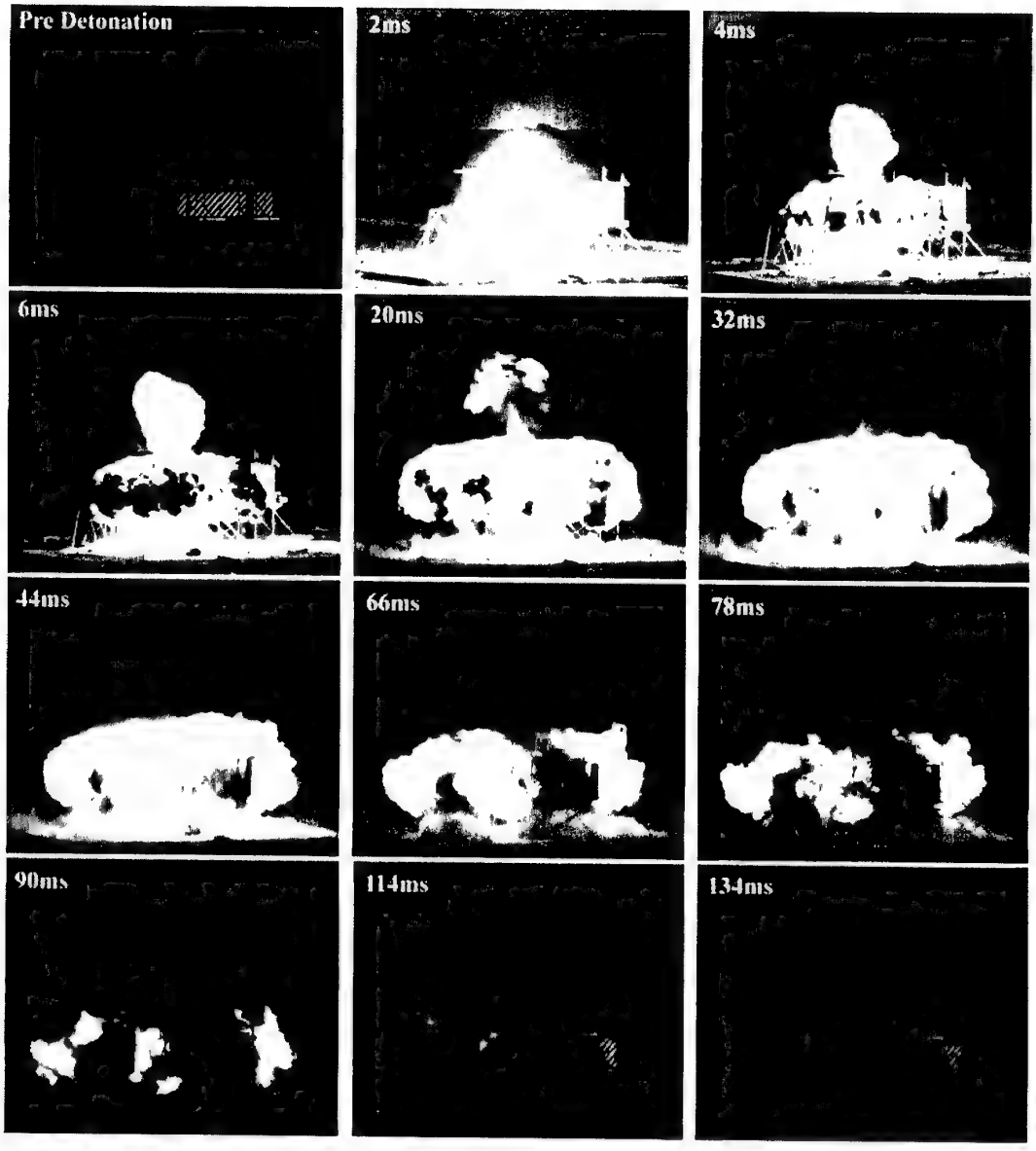

Figure 23. Fireball images recorded with a Locam.

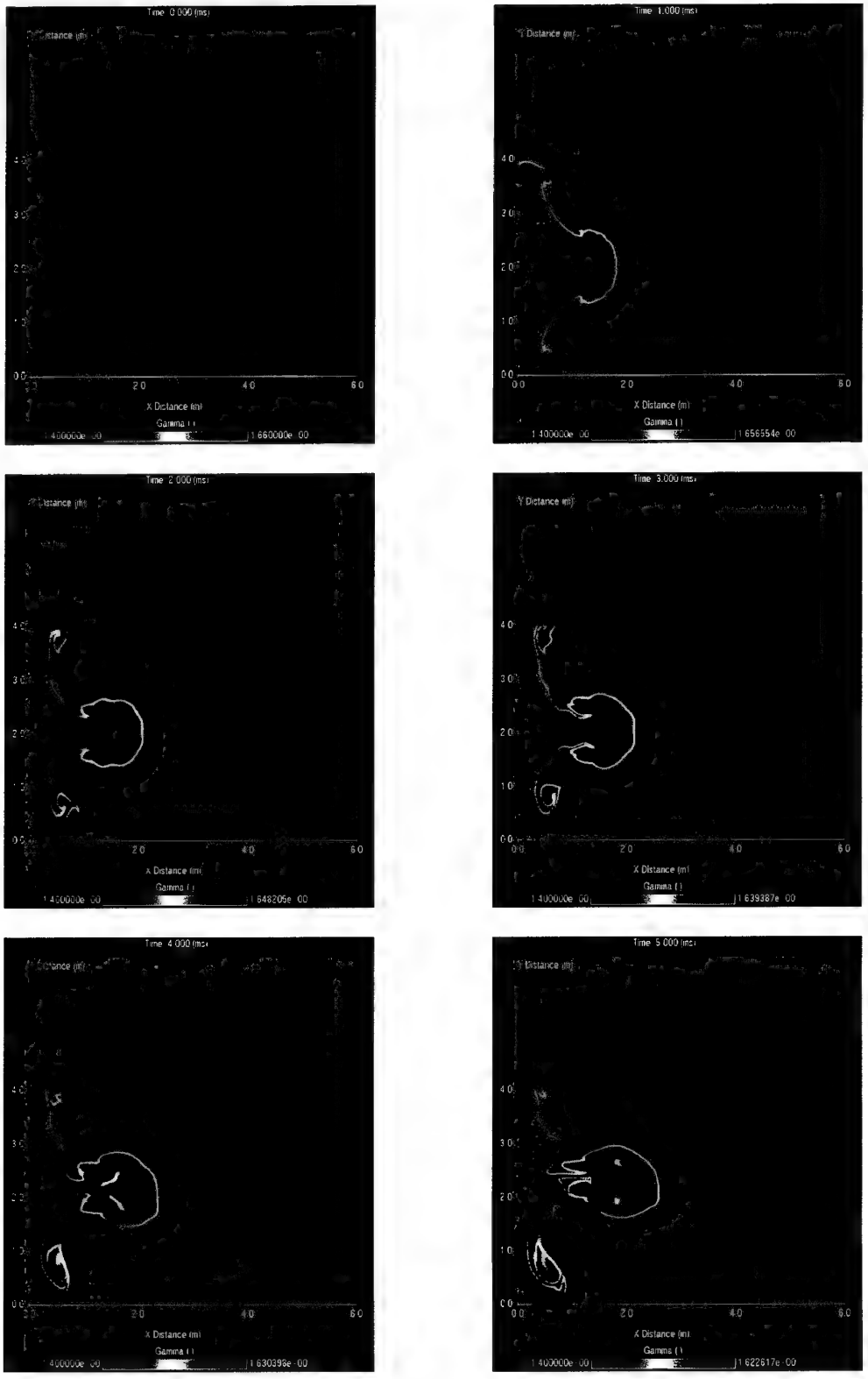

Figure 24. Contour plots of specific heat ratio for the cylindrical warhead.

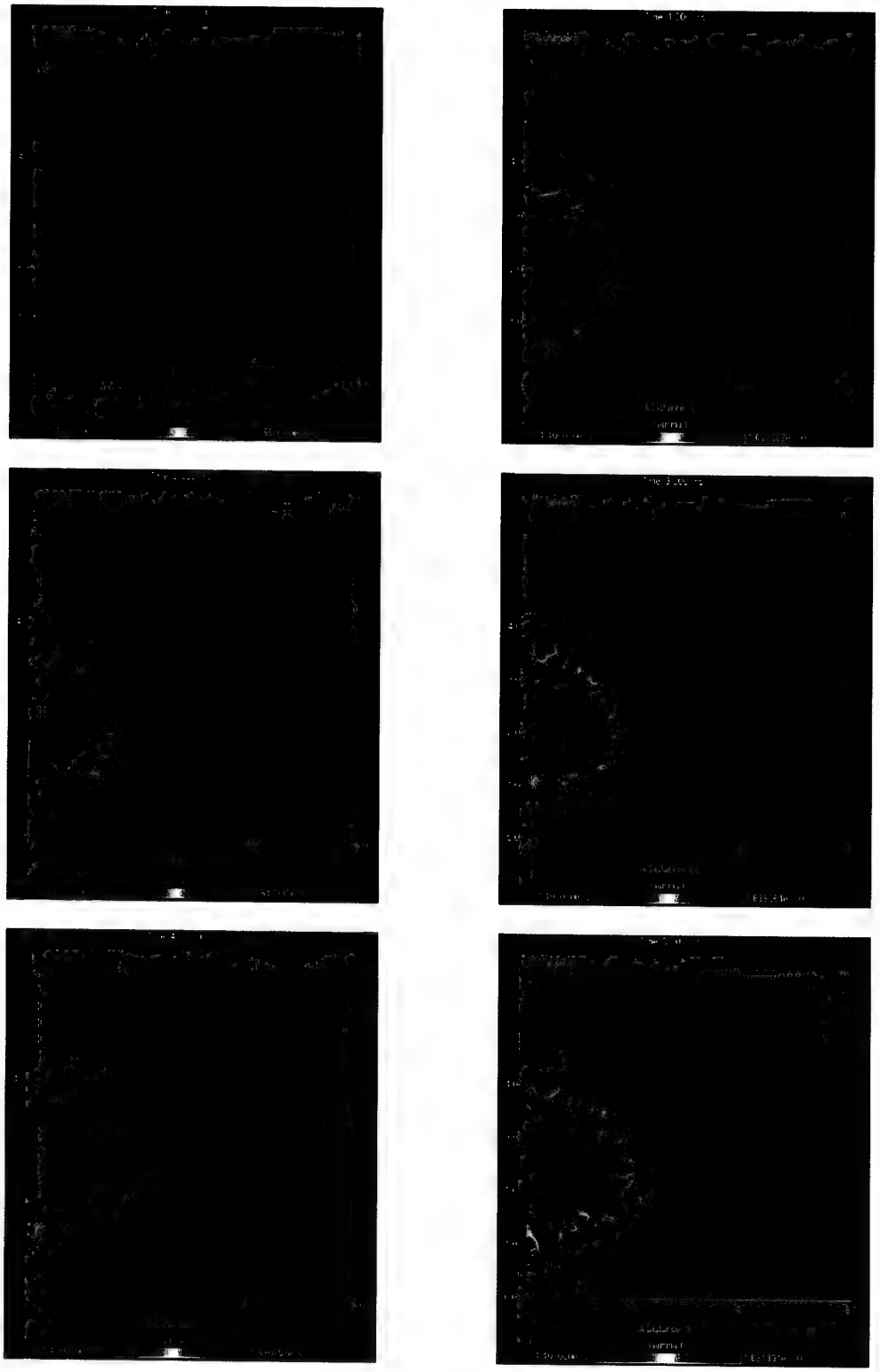

Figure 25. Contour plots of specific heat ratio for the spherical warhead.

5. Conclusion

An experimental and numerical investigation of the blast produced from a bare cylindrical high explosive warhead was conducted. Time of arrival measurements were used to determine peak overpressures in the near field. Overpressure histories in the mid to far field were measured with pressure gauges and also determined numerically. The results show significantly higher overpressures at points that are perpendicular to the axis of the cylindrical warhead. This feature of cylindrical warheads is important when determining the potential damage that can be caused by a warhead.

The results of the numerical analysis were used to generate two-dimensional contour plots of pressure. A close agreement was achieved with results from experiments for overpressures in the far field. In the mid field however, there were significant differences in the amplitudes of overpressures measured in the experiments and those determined with the numerical model. More work is needed in order to accurately model blast in the near to mid field. Currently, the numerical model is used to provide a qualitative comparison between a cylindrical and spherical warhead. The model shows that the blast waves differ in the mid field and become quite comparable in the far field.

6. Acknowledgments

The authors would like to thank, Trevor Delaney, Mick Footner, Dave Fraser, Jared Freundt, Dave Harris, Rob Hart, Des Kay, Blair Lade, Darren McQueen, Gordon Proctor, Ken Schebella, Max Joyner and Bob Arbon for their contributions to a successful field trial. They would also like to thank the staff at the Proof and Experimental Establishment Port Wakefield.

7. References

1. Lind, C.A., Cybyk, B.Z. and Boris, J.P., 1999, "Attenuation of Shock Waves by Geometrically Complex Objects", PVP-Vol. 396, Emerging Technologies in Fluids, Structures, and Fluid/Structure Interactions, ASME, pp. 231-239.

2. Ofengeim, D., K. and Drikakis, D., 1997, "Simulation of Blast Wave Propagation Over a Cylinder", Shock Waves Vol. 7, No. 5, pp. 305-317.

3. Varma, R.K., Tomar, C. P. S., Parkash, S. and Sethi, V.S., 1997, "Damage to Brick Masonry Panel Walls Under High Explosive Detonations", PVP-VOL. 351, Structures Under Extreme Loading Conditions, ASME, pp. 207-216.

4. Ismail, M.M. and Murray, S.G., 1993, "Study of the Blast Waves from the Explosion of Nonspherical Warheads, Propellants", Explosives, Pyrotechnics 18, pp. 132-138.

5. Zimmerman, H.D., Nguyen, C. T. and Hookham, P. A., 1999, "Investigation of Spherical vs Cylindrical Shape Effects on Peak Free-Air Overpressure and Impulse", Proceedings of 9th International Symposium on Interaction of the Effects of Munitions with Structures.

6. Held, M., 1991, "A simple Technique for Measuring the Blast Effect of Realistic Warheads", MABS-Symposium, pp. 731-740.

7. Rude, G., Boechler, D., Campbell, R. and Ritzel, D.V., 1994, "Blast Instrumentation at DRES", TTCP V/L (Sea) Workshop.

8. Wildegger-Gaissmaier, A.E., Matthews, K. and Katselis G., 1999, "Experimental and Computational Assessment of Blast and Fragmentation Characteristics of a Pre-fragmented Warhead LIMITED RELEASE", DSTO-TR-0755 Defence Science and Technology Organisation, AMRL.

9. Mitalas, R. and Harvey, R.B., 1958, "Peak Pressures from Distance/Time Data of an Expanding Spherical Shock Wave", Suffield Technical Paper No. 130, Suffield Experimental Station, Ralston Alberta.

10. Campbell, R. and Wilkinson, C., 2001, Photoinstrumentation for Warhead Characterisation, Terminal Effects Group Report, Weapons Systems Division, DSTO.

11. Ritzel, D.V. and Matthews, K., 1997, "An Adjustable Explosion-source Model for CFD Blast Calculations", ISSW21, 21st International Symposium on Shock Waves, Australia.

12. Brode, H.L., 1956, "The Blast Wave in Air Resulting from a High Temperature, High Pressure Sphere of Air (U)", RM-1825-AEC, The Rand Corp.

13. Kinney, G.F. and Graham, K.J., 1985, Explosive Shocks in Air, 2nd Edition, Springer-Verlag, New York.

14. Swisdak, M., 1975, "Explosion Effects and Properties Part 1 – Explosion Effects in Air", Naval Surface Weapons Centre, NSWC/WOL/TR 75-116.

15. Cooper, P. W., 1996, "Explosives Engineering", Wiley-VCH, Inc., ISBN 0-471-18636-8, pp. 23.

Appendix A: Side-on Overpressure Histories

The following overpressure histories were recorded during the Generic Warhead trial that was conducted from 12th to 22nd of June 2001. Four warheads were detonated during the trial. The warheads were cylindrical and made from Composition B. The nominal diameter, length and mass of each warhead was 141mm, 304 mm and 7.835kg, respectively. The warheads were placed with the length in the vertical direction and the horizontal centreline of the warhead was set at 2000 mm. In each figure below, the position of the pressure gauge is described in terms of the horizontal distance from the warhead centreline, X, and the vertical height, Y, from the ground (Y=0).

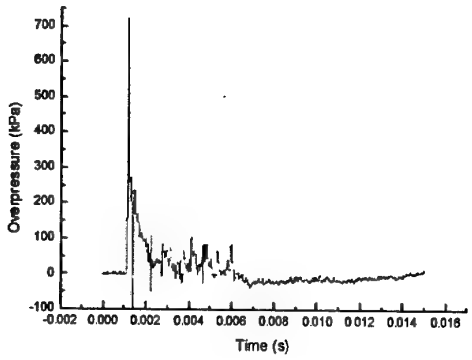

(a)

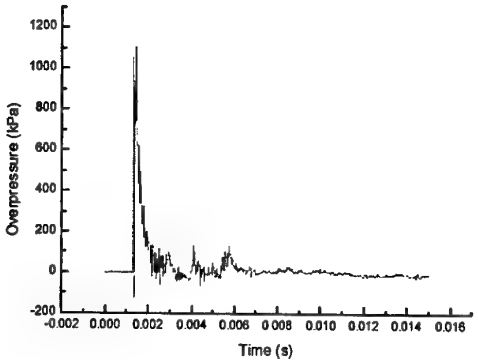

(b)

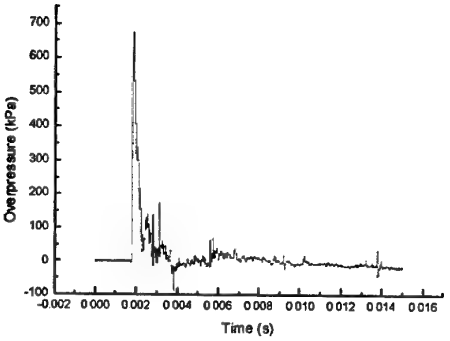

(c)

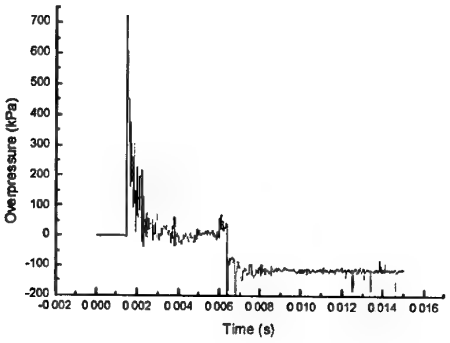

(d)

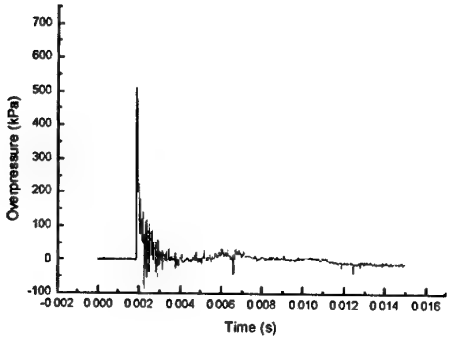

(e)

Experimental overpressure histories for Event 1. Gauge positions at (a) X=1945 mm and Y=1003 mm, (b) X=2525 mm and Y=1997 mm, (c) X=2950 mm and Y=2028 mm, (d) X= 2625 mm and Y=2600 mm and (e) X=3030 mm and Y=2582 mm.

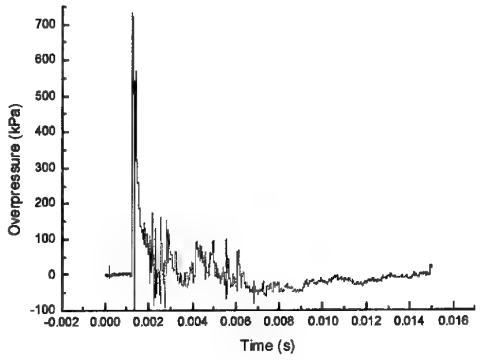

(a)

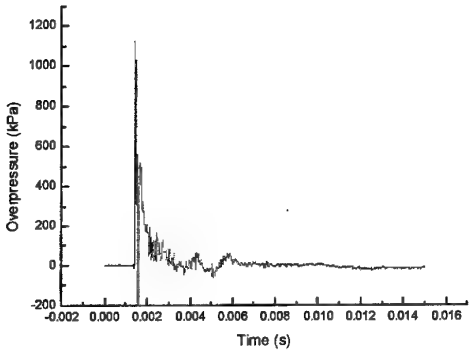

(b)

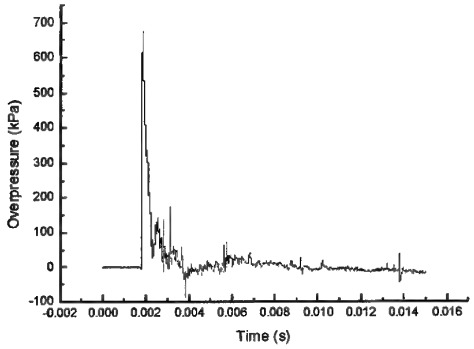

(b)

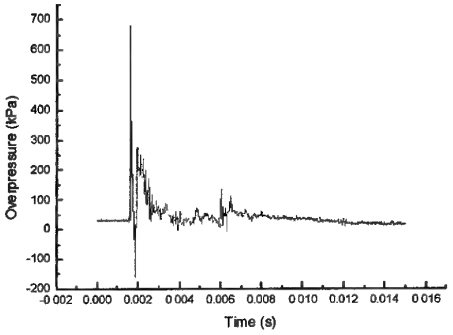

(d)

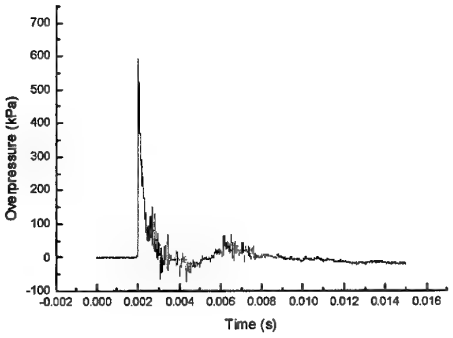

(e)

Experimental overpressure histories for Event 2. Gauge positions at (a) X=1993 mm and Y=1005 mm, (b) X=2520 mm and Y=2000mm, (c) X=2950 mm and Y=2035mm, (d) X= 2630 mm and Y=2600 mm and (e) X=3015 mm and Y=2585mm.

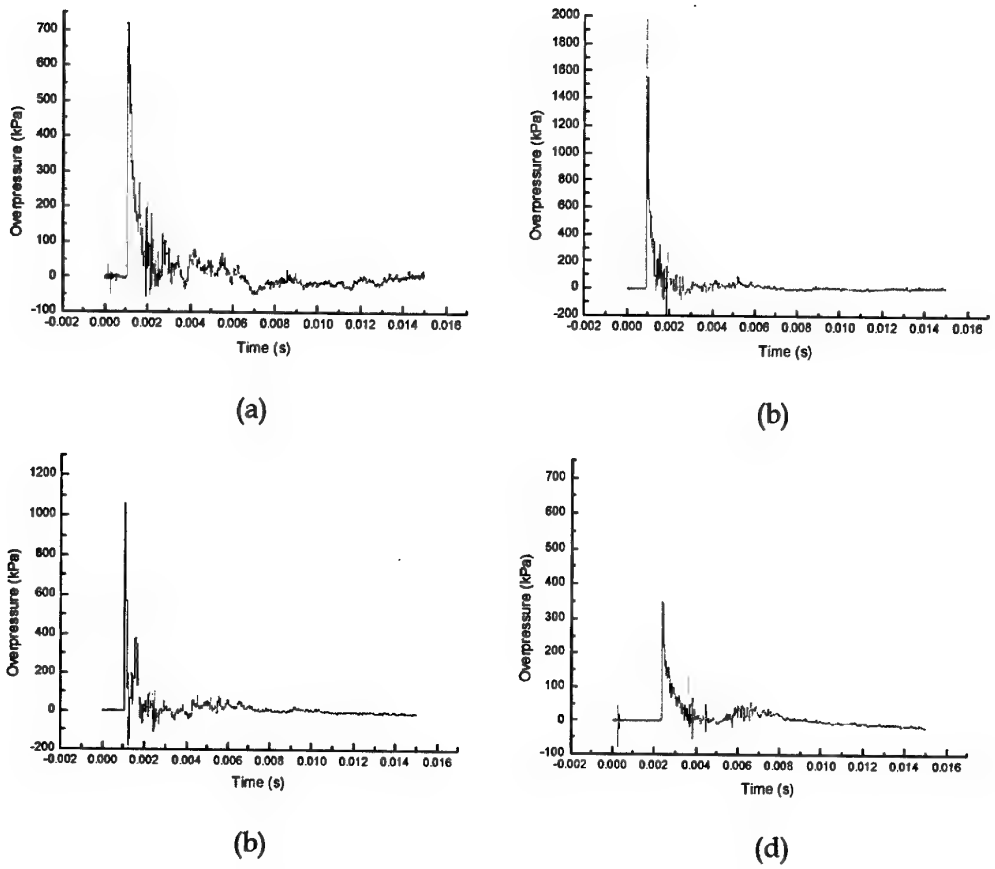

Experimental overpressure histories for Event 3. Gauge positions at (a) X=1790 mm and Y=994 mm, (b) X=1980 mm and Y=2010mm, (c) X=2090 mm and Y=2603 mm and (d) X= 3515 mm and Y=1995mm.

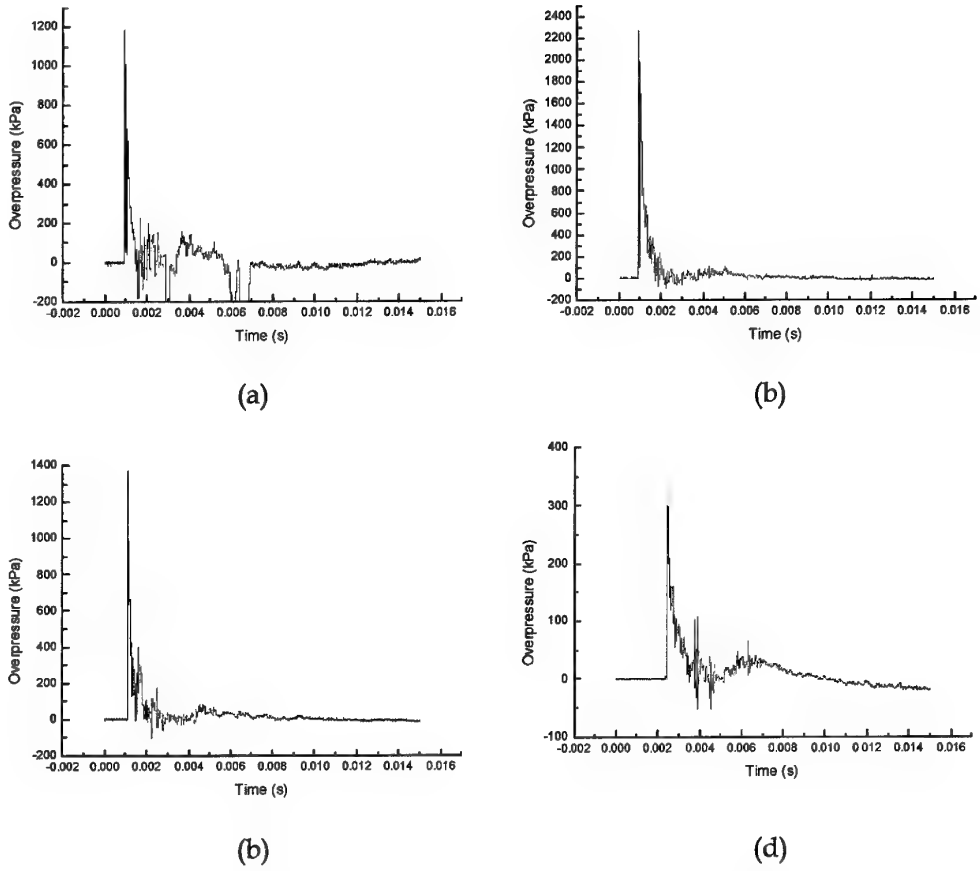

Experimental overpressure histories for Event 4. Gauge positions at (a) X=1431 mm and Y=987 mm, (b) X=2010 mm and Y=2013mm, (c) X=2125 mm and Y=2623 mm and (d) X= 3545 mm and Y=1993mm.

DISTRIBUTION LIST

Analysis of a Generic Warhead Part I:
Experimental and Computational Assessment of Free Field Overpressure

J.G. Anderson, G. Katselis and C. Caputo

AUSTRALIA

DEFENCE ORGANISATION

Task Sponsor

DGMD	copy 1
CMDR M. Uzzell ESSM Project Director	copy 2
SOAWW	copy 3

S&T Program

Chief Defence Scientist
FAS Science Policy
AS Science Corporate Management
Director General Science Policy Development
} shared copy

Counsellor Defence Science, London (Doc Data Sheet)
Counsellor Defence Science, Washington (Doc Data Sheet)
Scientific Adviser to MRDC Thailand (Doc Data Sheet)
Scientific Adviser Joint
Navy Scientific Adviser (Doc Data Sheet and distribution list only)
Scientific Adviser - Army (Doc Data Sheet and distribution list only)
Air Force Scientific Adviser
Director Trials

Systems Sciences Laboratory

Chief of Weapons Systems Division
Research Leader RLMWS
Head Dr. Anna Wildegger-Gaissmaier
Task Manager Dr. Peter Simms
Author(s): Dr. Jeremy Anderson
Mr. George Katselis
Mr. Carmine Caputo

DSTO Library and Archives

Library Fishermans Bend (Doc Data Sheet)
Library Edinburgh
Australian Archives

Capability Systems Staff

Director General Maritime Development (Doc Data Sheet only)
Director General Aerospace Development (Doc Data Sheet only)

Knowledge Staff

Director General Command, Control, Communications and Computers (DGC4) (Doc Data Sheet only)

Navy

SO (SCIENCE), COMAUSNAVSURFGRP, NSW (Doc Data Sheet and distribution list only)

Army

ABCA National Standardisation Officer, Land Warfare Development Sector, Puckapunyal (4 copies)

SO (Science), Deployable Joint Force Headquarters (DJFHQ) (L), Enoggera QLD (Doc Data Sheet only)

NPOC QWG Engineer NBCD Combat Development Wing, Puckapunyal, VIC (Doc Data Sheet relating to NBCD matters only)

Intelligence Program

DGSTA Defence Intelligence Organisation

Manager, Information Centre, Defence Intelligence Organisation

Defence Libraries

Library Manager, DLS-Canberra

Library Manager, DLS - Sydney West (Doc Data Sheet Only)

UNIVERSITIES AND COLLEGES

Australian Defence Force Academy

Library

Head of Aerospace and Mechanical Engineering

Serials Section (M list), Deakin University Library, Geelong, VIC

Hargrave Library, Monash University (Doc Data Sheet only)

Librarian, Flinders University

OTHER ORGANISATIONS

National Library of Australia

NASA (Canberra)

AusInfo

OUTSIDE AUSTRALIA

INTERNATIONAL DEFENCE INFORMATION CENTRES

US Defense Technical Information Center, 2 copies

UK Defence Research Information Centre, 2 copies

Canada Defence Scientific Information Service, 1 copy

NZ Defence Information Centre, 1 copy

ABSTRACTING AND INFORMATION ORGANISATIONS

Library, Chemical Abstracts Reference Service

Engineering Societies Library, US

Materials Information, Cambridge Scientific Abstracts, US

Documents Librarian, The Center for Research Libraries, US

INFORMATION EXCHANGE AGREEMENT PARTNERS

Acquisitions Unit, Science Reference and Information Service, UK
Library - Exchange Desk, National Institute of Standards and Technology, US

SPARES (5 copies)

Total number of copies: **47**

DEFENCE SCIENCE AND TECHNOLOGY ORGANISATION
DOCUMENT CONTROL DATA

1. PRIVACY MARKING/CAVEAT (OF DOCUMENT)

2. TITLE

Analysis of a Generic Warhead Part I:
Experimental and Computational Assessment of Free Field Overpressure

3. SECURITY CLASSIFICATION (FOR UNCLASSIFIED REPORTS THAT ARE LIMITED RELEASE USE (L) NEXT TO DOCUMENT CLASSIFICATION)

Document (U)
Title (U)
Abstract (U)

4. AUTHOR(S)

J.G. Anderson, G. Katselis and C. Caputo

5. CORPORATE AUTHOR

Systems Sciences Laboratory
PO Box 1500
Edinburgh South Australia 5111 Australia

6a. DSTO NUMBER	6b. AR NUMBER	6c. TYPE OF REPORT	7. DOCUMENT DATE
DSTO-TR-1313	AR-012-345	Technical Report	July 2002

8. FILE NUMBER	9. TASK NUMBER	10. TASK SPONSOR	11. NO. OF PAGES	12. NO. OF REFERENCES
9505 - 23 - 17	Nav 99/127	DGMD	38	15

13. URL on the World Wide Web

http://www.dsto.defence.gov.au/corporate/reports/DSTO-TR-1313.pdf

14. RELEASE AUTHORITY

Chief, Weapons Systems Division

15. SECONDARY RELEASE STATEMENT OF THIS DOCUMENT

Approved for public release

OVERSEAS ENQUIRIES OUTSIDE STATED LIMITATIONS SHOULD BE REFERRED THROUGH DOCUMENT EXCHANGE, PO BOX 1500, SALISBURY, SA 5108

16. DELIBERATE ANNOUNCEMENT

No Limitations

17. CASUAL ANNOUNCEMENT Yes

18. DEFTEST DESCRIPTORS

Blast overpressure, Blast waves, Blast effects, Antiship missiles

19. ABSTRACT

Experimental and numerical results are presented for the free field blast generated by a 7.8 kg cylindrical charge of Composition B high explosive. In the experiments, overpressure and shock front time of arrival measurements have been recorded. Overpressure measurements in the far field provide pressure histories at discrete locations. Peak overpressure in the near field is calculated from time of arrival measurements. In addition, the numerical model was used to generate overpressure histories and two-dimensional contour plots of the blast wave.